Signatures of Hydrometeor Species from Airborne Passive Microwave Data for Frequencies 10–183 GHz

[1]Daniel Cecil and [2]Kenneth Leppert II
[1]NASA Marshall Space Flight Center, Huntsville, Alabama
[2]Earth System Science Center, University of Alabama in Huntsville, Huntsville, Alabama

1. Introduction

- There are 2 basic precipitation retrieval methods using passive microwave measurements:
  1) Emission-based: Based on the tendency of liquid precipitation to cause an increase in brightness temperature (BT) primarily at frequencies below 22 GHz over a radiometrically cold background, often an ocean background (e.g., Spencer et al. 1989; Adler et al. 1991; McGaughey et al. 1996).
  2) Scattering-based: Based on the tendency of precipitation-sized ice to scatter upwelling radiation, thereby reducing the measured BT over a relatively warmer (usually land) background at frequencies generally ≥ 37 GHz (e.g., Spencer et al. 1989; Smith et al. 1992; Ferraro and Marks 1995).
- Passive microwave measurements have also been used to detect intense convection (e.g., Spencer and Santek 1985) and for the detection of hail (e.g., Cecil 2009; Cecil and Blankenship 2012; Ferraro et al. 2014).
- The Global Precipitation Measurement (GPM) mission expands upon the successful Tropical Rainfall Measurement Mission program to provide global rainfall and snowfall observations every 3 hours (Hou et al. 2014).
- One of the instruments on board the GPM Core Observatory is the GPM Microwave Imager (GMI) which is a conically-scanning microwave radiometer with 13 channels ranging from 10-183 GHz.
- Goal of this study: Determine the signatures of various hydrometeor species in terms of BTs measured at frequencies used by GMI by using data collected on 3 case days (all having intense/severe convection) during the Mid-latitude Continental Convective Clouds Experiment conducted over Oklahoma in 2011.

2. Method

- Data: Passive microwave BTs collected using the Advanced Microwave Precipitation Radiometer (AMPR) and Conical Scanning Millimeter-wave Imaging Radiometer (CoSMIR), dual-polarimetric radar data from the KVNX WSR-88D radar at Vance Air Force Base in Oklahoma.
- 3 case days were examined, including 22 April and 23-24 May 2011 (AMPR data available on 22 April and 24 May while CoSMIR data available on 23-24 May).
- Radar data was converted from its native polar coordinates to a Cartesian grid that stretched 600 by 600 km centered on KVNX and from the surface to a height of 16 km with a horizontal (vertical) resolution of 1.0 (0.5) km.
- Fuzzy-logic hydrometeor identification (HID) based on Liu and Chandrasekar (2000) and Dolan and Rutledge (2009) was applied to gridded radar data.
- To compare the HID with the passive microwave BTs, the passive microwave pixels closest to nadir were matched with vertical profiles of gridded KVNX data that occurred closest in time and space to each AMPR or CoSMIR pixel.
- To minimize the effect of the signal from one hydrometeor species dominating the signal from other species and better isolate the signal from each species separately, a subjective hierarchy of hydrometeor categories was applied. Each hydrometeor type was assigned a certain priority, and the type with the greatest priority in each profile was assigned to that column. The big drops category was given the highest priority followed by hail, high density graupel, low density graupel, rain, wet snow, aggregates, ice crystals (which were combined with vertically-oriented ice), and drizzle.

3. Overview

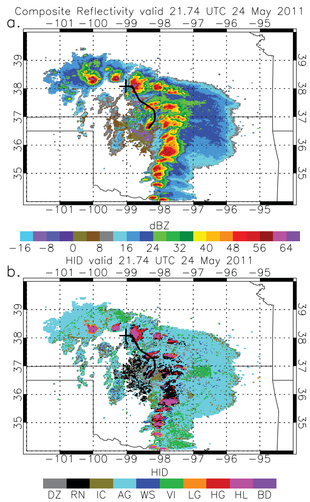

Figure 1. a) Composite gridded KVNX reflectivity valid at 2144 UTC 24 May 2011 and b) corresponding hydrometeor identification showing the hydrometeor with the greatest mass in each vertical column. The hydrometeors are drizzle (DZ), rain (RN), ice crystals (IC), aggregates (AG), wet snow (WS), vertically-oriented ice (VI), low density graupel (LG), high density graupel (HG), hail (HL), and big drops (BD). The black line in each panel indicates the location of the cross section shown in Fig. 2, and the plus symbol shows the start position of each cross section. The KVNX radar is located near the center of each panel.

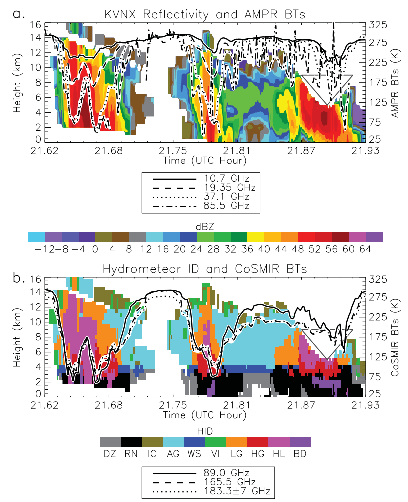

Figure 2. Cross section of a) gridded KVNX reflectivity along a 177-km ER-2 flight segment beginning at 2137 UTC 24 May 2011 and b) corresponding hydrometeor identification. The location of the cross section is shown in Fig. 1 by the black line, and the plus symbol corresponds to the left side of each cross section. The lines plotted over a) show the colocated AMPR BTs and over b) show the colocated CoSMIR BTs. Hydrometeor categories are the same as in Fig. 1, and the triangle in each panel represents the lack of radar coverage associated with the radar's cone of silence.

4. Frequency Distributions

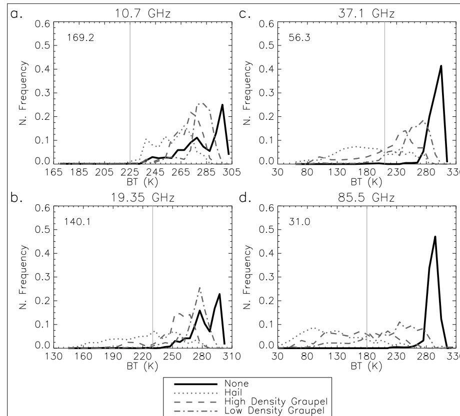

Figure 3. Normalized frequency distributions of vertical profiles containing hail, high density graupel, and low density graupel as a function of colocated a) 10-, b) 19-, c) 37-, and d) 85-GHz BT measured with AMPR on 22 April 2011 or 24 May 2011. The "none" category includes profiles without any valid hydrometeor identification. For a) and b), the BT bin size is 10 (5) K to the left (right) of the thin vertical line. For c) and d) the bin size is 20 (10) K to the left (right) of the thin vertical line. The minimum BT measured at each frequency for the shown hydrometeor species is indicated by the number in the top left corner of each panel.

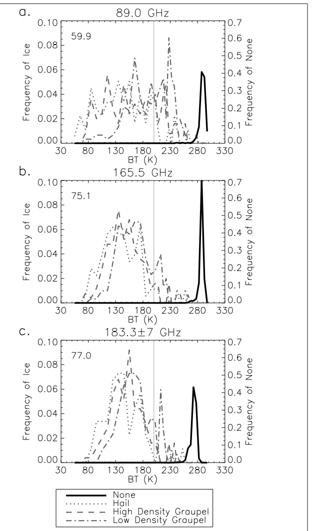

Figure 4. Normalized frequency distributions of vertical profiles containing hail, high density graupel, low density graupel, and no valid hydrometeor identification (none) as a function of colocated a) 89-, b) 165-, and c) 183-GHz BT measured with CoSMIR on 23–24 May 2011. The BT bin size is 10 (5) K to the left (right) of the thin vertical line in each panel. The values along the left (right) side of the plot correspond to the hail and graupel (none) categories. The minimum BT measured at each frequency for the shown hydrometeor species is indicated by the number in the top left corner of each panel.

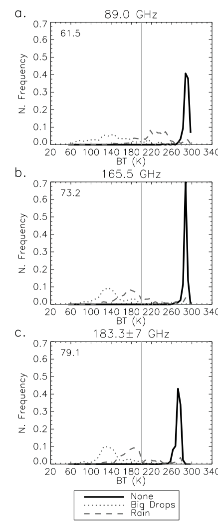

Figure 5. As in Fig. 4, except for profiles containing big drops, rain, and profiles containing no valid hydrometeor identification.

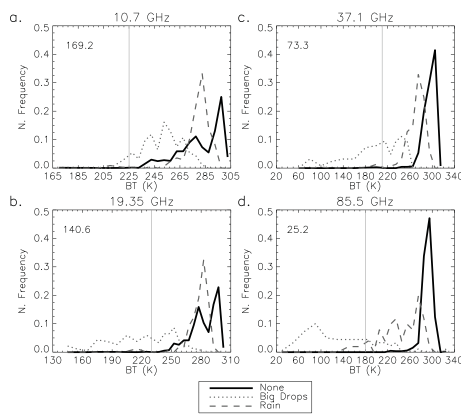

Figure 6. As in Fig. 3, except for profiles containing big drops, rain, and profiles containing no valid hydrometeor identification.

5. Probability

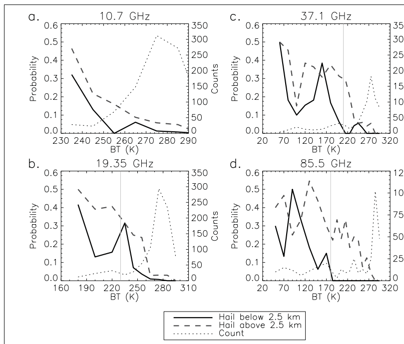

Figure 7. Probability of the occurrence of hail at low levels (i.e., ≤2.5 km) or at upper levels (i.e., >2.5 km) in a vertical column as a function of colocated AMPR BT at a) 10, b) 19, c) 37, and d) 85 GHz for data collected on 22 April or 24 May 2011. The BT bin size in a) is 10 K. In b) through d) the BT bin size is 20 (10) K to the left (right) of the thin vertical line. Note that the hydrometeor hierarchy was not applied to this or subsequent figures.

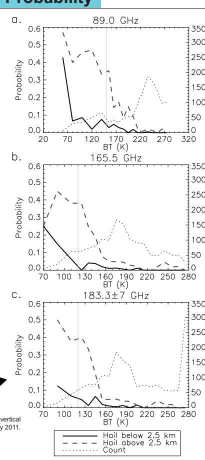

Figure 8. Probability of the occurrence of hail at low levels (i.e., ≤2.5 km) or at upper levels (i.e., >2.5 km) in a vertical column as a function of colocated CoSMIR BT at a) 89, b) 165, and c) 183 GHz for data collected on 23–24 May 2011. The BT bin size is 20 (10) K to the left (right) of the thin vertical line in each panel.

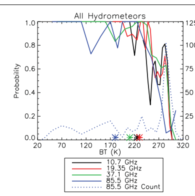

Figure 9. Probability of a non-zero mass of any hydrometeor type at low levels (≤ 2.5 km height) as a function of colocated AMPR BT at various frequencies for data collected on 22 April or 24 May 2011. The blue dotted line shows the number of profiles in each 85-GHz BT bin as indicated by the axis on the right side of the figure (counts for other frequencies are not shown for clarity). The colored asterisks at the bottom of the figure indicate the BT at which the bin sizes change for each frequency, and bin sizes relative to each symbol are the same as in Fig. 3.

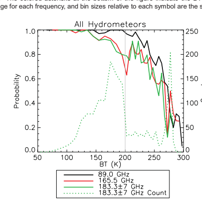

Figure 10. Probability of a non-zero mass of any hydrometeor type at low levels (≤ 2.5 km height) as a function of colocated CoSMIR BT at various frequencies for data collected on 23−24 May 2011. The green dotted line shows the number of profiles in each 183-GHz BT bin as indicated by the axis on the right side of the figure (counts for other frequencies are not shown for clarity). To the left (right) of the thin vertical line, the BT bin size is 10 (5) K.

6. Conclusions

- Hail is associated with a strong scattering signature at all frequencies examined, including 10 GHz.
- Frequencies ≤ 37 GHz show the strongest distinction between hail and other hydrometeor types.
- Low-level hail becomes probable for a BT below 240 K at 19 GHz, 170 K at 37 GHz, 90 K at 85 GHz, 80 K at 89 GHz, 100 K at 165 GHz, and 100 K at 183 GHz.
- Graupel may be distinguished from hail and profiles without any hydrometeor species by its strong scattering signature at higher frequencies (e.g., 165 GHz) and its relative lack of scattering at frequencies ≤ 19 GHz.
- Liquid precipitation can be best distinguished from no-rain profiles over land when associated above with hail and/or graupel (hydrometeor species with a strong ice scattering signature).
- Probability of surface precipitation becomes very likely (~100%) for a BT below 230 K at 10 GHz, 250 K at 19 GHz, 240 K at 37 GHz, 230 K at 85 GHz, 220 K at 89 GHz, 140 K at 165 GHz, and 140 K at 183 GHz.
- Note that these results are valid over intense convection for a few days over Oklahoma in spring 2011 (sample size is small).

7. References

- Adler, R. F., H.-Y. M. Yeh, N. Prasad, W.-K. Tao, and J. Simpson, 1991: Microwave simulations of a tropical rainfall system with a three-dimensional cloud model. *J. Appl. Meteor.*, **30**, 924–953.
- Cecil, D. J., 2009: Passive microwave brightness temperatures as proxies for hailstorms. *J. Appl. Meteor. Climatol.*, **48**, 1281–1286.
- Cecil, D. J., and C. B. Blankenship, 2012: Toward a global climatology of severe hailstorms as estimated by satellite passive microwave imagers. *J. Climate*, **25**, 687–703.
- Dolan, B., and S. A. Rutledge, 2009: A theory-based hydrometeor identification algorithm for X-band polarimetric radars. *J. Atmos. Oceanic Technol.*, **26**, 2071–2088.
- Ferraro, R. R., and G. F. Marks, 1995: The development of SSM/I rain-rate retrieval algorithms using ground-based radar measurements. *J. Atmos. Oceanic Technol.*, **12**, 755–770.
- Ferraro, R. R., J. Beauchamp, D. J. Cecil, and G. M. Heymsfield, 2014: A prototype hail detection algorithm and hail climatology developed with the Advanced Microwave Sounding Unit (AMSU). *Atmos. Res.*, submitted.
- Hou, A. Y., R. K. Kakar, S. Neeck, A. A. Azarbarzin, C. D. Kummerow, M. Kojima, R. Oki, K. Nakamura, and T. Iguchi, 2014: The Global Precipitation Measurement (GPM) mission. *Bull. Amer. Meteor. Soc.*, in press.
- Liu, H., and V. Chandrasekar, 2000: Classification of hydrometeors based on polarimetric radar measurements: Development of fuzzy logic and neuro-fuzzy systems, and in situ verification. *J. Atmos. Oceanic Technol.*, **17**, 140–164.
- McGaughey, G., E. J. Zipser, R. W. Spencer, and R. E. Hood, 1996: High-resolution passive microwave observations of convective systems over the tropical Pacific Ocean. *J. Appl. Meteor.*, **35**, 1921–1947.
- Smith, E. A., H. J. Cooper, X. Xiang, A. Mugnai, and G. J. Tripoli, 1992: Foundations for statistical-physical precipitation retrieval from passive microwave satellite measurements. Part I: Brightness temperature properties of a time-dependent cloud-radiation model. *J. Appl. Meteor.*, **31**, 506–531.
- Spencer, R. W., and D. A. Santek, 1985: Measuring the global distribution of intense convection over land with passive microwave radiometry. *J. Climate Appl. Meteor.*, **24**, 860–864.
- Spencer, R. W., H. M. Goodman, and R. E. Hood, 1989: Precipitation retrieval over land and ocean with the SSM/I: Identification and characteristics of the scattering signal. *J. Atmos. Oceanic Technol.*, **6**, 254–273.

Acknowledgement: Funding for this research was generously provided through the NASA Precipitation Measurement Missions Science Team.